

Vibrational Quantum States of Methanol

Ayaki Sunaga,¹ Tibor Györi,^{2,*} Gábor Czakó,^{2,†} and Edit Mátyus^{1,‡}

¹*ELTE, Eötvös Loránd University, Institute of Chemistry,
Pázmány Péter sétány 1/A 1117 Budapest, Hungary*

²*MTA-SZTE Lendület “Momentum” Computational Reaction Dynamics Research Group,
Interdisciplinary Excellence Centre and Department of Physical Chemistry and Materials Science,
Institute of Chemistry, University of Szeged,
Rerrich Béla tér 1, Szeged H-6720, Hungary.*

(Dated: May 23, 2025)

The methanol molecule is a sensitive probe of astrochemistry, astrophysics, and fundamental physics. The first-principles elucidation and prediction of its rotation-torsional-vibrational motions are enabled in this work by the computation of a full-dimensional, *ab initio* potential energy surface (PES) and numerically exact quantum dynamics. An active-learning approach is used to sample explicitly correlated coupled-cluster electronic energies, and the datapoints are fitted with permutationally invariant polynomials to obtain a spectroscopic-quality PES representation. Variational vibrational energies and corresponding tunnelling splittings are computed up to the first overtone of the C-O stretching mode by direct numerical solution of the (ro)vibrational Schrödinger equation with optimal internal coordinates and efficient basis and grid truncation techniques. As a result, the computed vibrational band origins finally agree with experiment within 5 cm^{-1} , allowing for the exploration of the large-amplitude quantum mechanical motion and tunnelling splittings coupled with the small-amplitude vibrational dynamics. These developments open the route towards simulating rovibrational spectra used to probe methanol in outer space and in precision science laboratories, as well as for probing interactions with external magnetic fields.

CONTENTS

I. Introduction	2
II. Construction of the potential energy surface	3
A. Background and methodology	3
B. Properties and validation of the final PES	4
III. Variational vibrational computations	6
A. Methodological details	6
B. Vibrational energies	8
IV. Summary, conclusion, and outlook	11
Acknowledgments	11
References	11

* tibor.gyori@chem.u-szeged.hu

† gczako@chem.u-szeged.hu

‡ edit.matyus@ttk.elte.hu

I. INTRODUCTION

CH₃OH is the smallest alcohol and a prototype of quantum mechanical large-amplitude motions and corresponding tunnelling splittings. It is also one of the most abundant organic molecules in the Universe, which explains its importance in astrophysics. Its particular rovibrational level structure, dominated by the large-amplitude internal rotation, has been proposed as a sensitive probe for the proton-to-electron mass ratio variation at astronomical scales¹⁻⁴. Most recently, the internal rotation of substituted methanol compounds was considered for enhanced parity-violating effects⁵. The hyperfine-Zeeman splittings of methanol, based on a reduced dimensionality model, were used to measure (weak) magnetic fields on distant astronomical objects⁶. The methanol molecule also plays a central role in astrochemistry; the ratio of its isotopologues has been studied in the context of the formation of organic compounds in outer space⁷⁻¹².

Methanol has been a prototype for fundamental spectroscopy and quantum nuclear motion theory, mostly for the non-trivial couplings of its small-amplitude degrees of freedom, the large-amplitude internal rotation, and the overall molecular rotation. Its fundamental vibrations were detected with infrared¹³ and Raman¹⁴ spectroscopy already in 1937-38 and were assigned based on the C_s point group¹⁵⁻¹⁹. The torsion-rotation coupling was later analysed in a series of work²⁰⁻²⁵, recently followed by high-precision spectroscopy using an ultra-narrow quantum cascade laser²⁶. The molecular symmetry group²⁷ can be used for a more complete understanding of the degenerate and tunnelling splitting levels, but arguments were put forward for using the complete permutation-inversion group^{28,29}, so as not to lose important parity information of the eigenstates.

We also note that combination bands of methanol have been studied with matrix isolation spectroscopy³⁰⁻³². Regarding (rectilinear) normal coordinate computations, which are limited to describing small-amplitude vibrations, we mention vibrational self-consistent field (VSCF) and related vibrational configuration interaction-type (VCI) computations³³⁻³⁷. The computed VCI fundamental-mode energies, not considering the torsional motion and the tunneling splittings, agree well with the matrix isolation data³⁸. Further computational methodologies were developed using a tree-tensor-network-state ansatz based on the state-shifted Hamiltonian³⁹.

There has been recent progress in a numerically exact solution of the rovibrational Schrödinger equation on an *ab initio* (or perhaps spectroscopically refined) potential energy surface (PES), allowing also for large-amplitude motions (LAMs)⁴⁰⁻⁴⁴. In scaling up the vibrational dimensionality, we mention recent developments in collocation^{45,46} and contraction⁴⁷⁻⁴⁹. The full-dimensional (12D) variational computation of methanol was first reported by Lauvergnat and Nauts^{50,51}. In our group, 12D variational computations were also performed using the GENIUSH-Smoljak approach for methane-atom(ion) complexes⁵²⁻⁵⁵, by including the atom(ion)-methane large-amplitude relative motions fully coupled with the methane's small-amplitude internal vibrations. These developments were followed by applications for the formic acid molecule^{56,57} and methanol⁵⁸ using path-following curvilinear normal coordinates. The efficient basis and grid truncation made it possible to converge the vibrational energies of methanol (12D) within 1-2 cm⁻¹ with respect to the vibrational basis and grid up to the combination bands at ca. 2200 cm⁻¹ beyond the zero-point vibrational energy, ZPVE. In this range, the large, 10-20 cm⁻¹ deviation from experiment indicated that the underlying PES⁵⁹ (henceforth labeled as PES13) required improvement⁵⁸.

Regarding the PES development, the challenging aspects of treating the torsional motion are (i) accounting for the three equivalent minima and (ii) covering a wider geometry region beyond small-amplitude motions (SAMs) about local minima. A solution for (i) has been well established in the community: the permutation-invariant-polynomial (PIP) method, which was initially reported by Joel Bowman's group⁶⁰⁻⁶² and is continuing to see recent improvements⁶³⁻⁶⁷. Solving (ii) involves expanding the region of interest in the 12D hypervolume, which necessitates the use of either increasingly many *ab initio* energies to adequately sample the hypervolume or some sparse sampling technique that takes advantage of the fitting method's ability to interpolate between the points of the fitting set. Since high-accuracy *ab initio* energies are computationally expensive, the latter approach is preferable, but the practical implementation details remain challenging to be tackled in this work.

One of the strategies for efficiently choosing geometry points for the fitting is the active-learning-like approach of the ROBOSURFER program system⁶⁸. The accuracy of PESs developed with the PIP fitting has been demonstrated^{54,55} from the equilibrium structures up to the methane-atom(ion) dissociation limits of the methane complexes CH₄·Ar and CH₄·F⁻, of which the latter applications used ROBOSURFER. In this study, we use and improve upon this combination of

methods to obtain a new PES for methanol, which is reported in the first part of the paper.

II. CONSTRUCTION OF THE POTENTIAL ENERGY SURFACE

A. Background and methodology

The concept of a PES arises from the Born-Oppenheimer approximation. For every molecular geometry, there is a potential energy value that can (in principle) be obtained by solving the Schrödinger equation of the electrons. While no analytical solution is known for many-electron systems and numerically exact solutions are unfeasible in most cases, modern quantum chemistry offers a number of efficient and accurate approximations. These typically involve the simultaneous use of: (I) an approximate many-electron wavefunction where the correlated motion of electrons stemming from electron-electron repulsion is only partially considered and relativistic effects are either ignored or approximated, and (II) a finite set of carefully optimized basis functions which are linearly combined to construct the molecular orbitals.

In this study, we combine a well-established coupled-cluster approximation of electronic motion, CCSD(T)-F12b⁶⁹, with the cc-pVTZ-F12⁷⁰ basis set to compute potential energy values at a reasonable computational cost.

In principle, a variational vibrational computation could be carried out by querying the *ab initio* energy computation method described above at every quadrature point of the numerical integration grid used for computing the matrix elements of the vibrational Hamiltonian. But in practice, this would be prohibitively slow, as the potential energy is required at (hundreds of) millions of geometries, and every *ab initio* energy may take a couple of minutes of CPU time. Therefore, to make the *ab initio* computation of (ro)vibrational energy levels possible, another layer of approximation needs to be introduced: a surrogate model PES, fitted to a limited number of *ab initio* energies.

In this study, we use the Braams–Bowman implementation of permutationally invariant polynomials (PIP)⁶¹ for fitting. Briefly, the polynomials are expanded in terms of Morse variables

$$y_{ij} = \exp(-r_{ij}/a), \quad (1)$$

where r_{ij} is the distance between atoms i and j and a is a distance transformation parameter. The number of coefficients (and as a result, the flexibility of the fitting function) is primarily controlled by limiting the degrees of the polynomials, as per standard practice. The energy expression of the PES is

$$E = \sum_{k=1}^Z c_k T_k M_k, \quad (2)$$

where Z is the number of permutationally invariant monomials, while c_k and T_k are the coefficient and monomial prefactor of the k -th monomial M_k , respectively. The PIP method ensures that the values of the energy returned by the PES function are invariant to any permutation of like atoms, in our case, all four H-atoms. A special feature of the PIP implementation used in this study is the ability to increase the fitting function flexibility by adding extra polynomials that are restricted in the number of atomic positions they are permitted to depend on. We call these ‘extra q -body polynomials’, and we employ extra 2-, 3-, and 4-body polynomials in the functional form of our new PES. These extra polynomials and the main polynomial can each use different values for a , Eq. (1), to achieve optimal fitting of the *ab initio* energy-geometry pairs in the fitting set. The polynomial coefficients are obtained through weighted linear least squares (LLS) fitting; the weighting function is provided in Eq. S3 of the ESI.

For constructing the fitting set, we used the ROBOSURFER program system⁶⁸, and for computing the required *ab initio* energies, we used the Molpro^{71–74} quantum chemistry package. Without going into the details of its operation, ROBOSURFER automates the development of PESs through an iterative, active-learning-like process, which gradually expands the fitting set with additional samples (geometry-energy pairs) until the quality of the fitted PES is judged to be satisfactory.

For the PES development, we have taken the approach of starting with a small fitting set, low degree polynomials, a high threshold (in terms of weighted error) for adding new geometries to the

fitting set (E_{targ}), and gradually increasing both the flexibility of the fitting function and the accuracy we demand from the PES, as the fitting set grew. In addition to readjusting the parameters of the automated PES development process multiple times, we have also, on a handful of occasions, manually injected geometries into the development process, which were sampled around outliers in the fit. The PES development was started from a fitting set of 530 geometries, $E_{\text{targ}} = 1$ kcal/mol (349.8 cm^{-1}), a 4th degree polynomial fit and no extra monomials, resulting in 317 polynomial coefficients. By the end of the PES development, the fitting set grew to 39 401 geometries, E_{targ} was lowered to 0.05 kcal/mol (17.5 cm^{-1}), and the complexity of the fitting function was increased to the state shown in Table I. Further details of the fitting and PES development methods, as well as a highly detailed account of the progress of PES development and fitting error minimisation efforts, are provided in Section S1 of the ESI.

B. Properties and validation of the final PES

Our new PES, named PES25, is the result of fitting the final geometry set of 39 401 points with the PIP method and the parameters shown in Table I, yielding 9652 polynomial coefficients. For numerical stability reasons discussed in Section S2 of the ESI, we obtained the final coefficient values of PES25 using the DGELSY linear least squares solver, which is a LAPACK subroutine⁷⁵. This results in slightly higher fitting errors, but produces a PES with smoother derivatives.

TABLE I. Employed distance transformation parameters and polynomial degrees in the fitting function

Polynomial	degree	a [bohr]
main (6-body)	7	1.9
extra 2-body	2	2.5
extra 3-body	3	1.7
extra 4-body	4	3.0

Our fidelity assessment of the fit is summarised in Table II. The RMS fitting error of PES25 over its fitting set, 27.3 cm^{-1} , is noticeably higher than those of our previous spectroscopic PIP-PESs; e.g., the RMSEs of Refs 54 and 55 are ca. 1 cm^{-1} and 3 cm^{-1} , respectively. While the RMS weighted fitting error of PES25 is considerably better at 17.3 cm^{-1} , that is still an order of magnitude larger than the errors of the aforementioned PESs. This is attributable to a multitude of factors.

TABLE II. Assessment of PES25: number of geometries, root-mean-square error (RMSE) of the fitting set, for energy ranges relative to the *ab initio* equilibrium energy. The total RMSE and the RMS weighted error (RMSWE) over all geometry points are also listed.

Energy range [cm^{-1}]	# of geometries	RMSE [cm^{-1}]
0–13000	29029	13.8
13000–22000	7587	36.9
22000–44000	2785	69.8
Total points	39401	
Total RMSE		27.3
Total RMSWE		17.3

First, it is generally perilous to judge the quality of a statistical model (such as a fitted PES) only from its error over its fitting set, as the accuracy of the model can be vastly different at different geometries. This is illustrated by the fact that over the course of developing this PES we have accumulated over 174 000 geometries which were not included in the fit due to their weighted fitting error being less than 17.5 cm^{-1} . While this is still not a statistically independent test set, it does imply that the PES works well even for geometries not included in the fitting set.

Second, there are matters of geometry generation. The $\text{CH}_4\cdot\text{Ar}$ PES in Ref. 54 was developed before the development of ROBOSURFER, and its fitting set was generated through the random distortion of methane’s equilibrium geometry, while the C–Ar distance and CH_4 orientation were

randomly sampled. Since this was done without any steps to filter out geometries that would have already been well-described by the PES without them, it is likely that the RMS fitting error of the fitting set of Ref. 54 benefited from the sampling method. While the PES reported in Ref. 55 was developed with ROBOSURFER, PES25 is the result of far more sampling effort, which almost always raises the RMS errors of the fitting set, as it discovers and adds points of high error into the fit.

TABLE III. Geometries at one of the three permutationally equivalent equilibrium structures and one saddle point obtained with PES13⁵⁹ and PES25 (this work) and *ab initio* computations. Bond lengths are in Å, bond angles are in degrees. The internal coordinates r , θ , and τ are defined in Fig. 1.

	Equilibrium structure				Saddle point			
	this work		Ref. 59		this work		Ref. 59	
	PES25	<i>ab initio</i> ^a	PES13	<i>ab initio</i> ^b	PES25	<i>ab initio</i> ^a	PES13	<i>ab initio</i> ^b
$r_1(\text{CO})$	1.4196	1.4199	1.419	1.422	1.4236	1.4235	1.423	1.423
$r_2(\text{OH})$	0.9583	0.9582	0.959	0.959	0.9558	0.9560	0.957	0.956
$r_3(\text{CH}_1)$	1.0876	1.0875	1.089	1.088	1.0908	1.0910	1.094	1.093
$r_{4,5}(\text{CH}_n, n = 2, 3)$	1.0931	1.0931	1.095	1.095	1.0909	1.0907	1.093	1.093
$\theta_1(\text{HOC})$	108.19	108.20	108.3	108.6	108.68	108.65	109.1	108.7
$\theta_2(\text{COH}_1)$	106.65	106.74	106.7	106.8	112.05	112.04	112.7	112.1
$\theta_{3,4}(\text{COH}_n, n = 2, 3)$	111.94	111.90	111.9	112.0	109.50	109.49	109.4	109.5
$\tau_1(\text{H}_1\text{COH})$	180.00	180.00	180.0	180.0	0.00	0.00		
$\tau_2(\text{H}_2\text{COH})$	61.39	61.39			-120.37	-120.39		
$\tau_3(\text{H}_3\text{COH})$	298.61	298.61			120.37	120.39		

^a CCSD(T)-F12b/cc-pVTZ-F12 ^b CCSD(T)-F12b/aug-cc-pVDZ

Third, the weighting function (Eq. S3 in the ESI) used for PES25 to fit the surface and select the geometries places much more importance on moderately high-energy geometries than the two previous PESs. As an example, while the development of PES25 considered all geometries up to 13 011 cm^{-1} equally important (a reasonable guess for a PES intended to describe vibrations up to ZPVE + 2200 cm^{-1}), the weighting used in Ref. 55 would have only given a geometry at 13 011 cm^{-1} a weight of ~ 0.4 . As a result of this increased region of interest (in terms of energy), achieving a low RMS fitting error becomes much more challenging and demands more flexibility from the fitting function. And finally, of course, different molecular systems can be more or less challenging to create a PES for. It is possible that methanol is inherently a more difficult system to fit than $\text{CH}_4\cdot\text{Ar}$ or $\text{CH}_4\cdot\text{F}^-$.

The quality and improvement of PES25 over PES13 can also be assessed by comparing the *ab initio* computations and the literature values of Ref. 59. The molecular structure parameters are listed in Table III. The PES25 values agree well with the *ab initio* values with a maximum deviation of 3×10^{-4} Å for bond lengths and 0.09° for bond angles. The largest changes due to our larger basis set, which are obtained from the comparison between the *ab initio* values computed in this study and Ref. 59, are 2×10^{-3} Å for bond lengths and 0.4° for bond angles, respectively. The accuracy of the PES fitting is sufficient to reflect the improvement in terms of the basis set size.

The harmonic frequencies and deviations from the *ab initio* computations are summarised in Table IV. Both MAE and MAX errors of PES25 are less than those of Ref. 59. Most of the harmonic frequencies obtained with the two *ab initio* computations agree within a few cm^{-1} , and the largest deviation of more than 6.0 cm^{-1} is found for the modes related to the H-C-O- H_n ($n = 1, 2, 3$) dihedral angles. Interestingly, the torsional harmonic frequency changes by more than 10 cm^{-1} by changing from PES13 to PES25. However, most of the variational vibrational energies corresponding to the torsional motion are less sensitive to this change (Table S6 of the ESI). The largest deviation, 8.3 cm^{-1} , is observed in the 1800 cm^{-1} region beyond the ZPVE (Table S7 of the ESI).

As a final test of the quality of PES25, we have prepared one-dimensional slices of the PES along selected internal coordinates, which extend into regions moderately far from the equilibrium structure. As shown in Figs. S11–S13 of the ESI, the fitting errors along these slices match the RMS weighted fitting error of the fitting set.

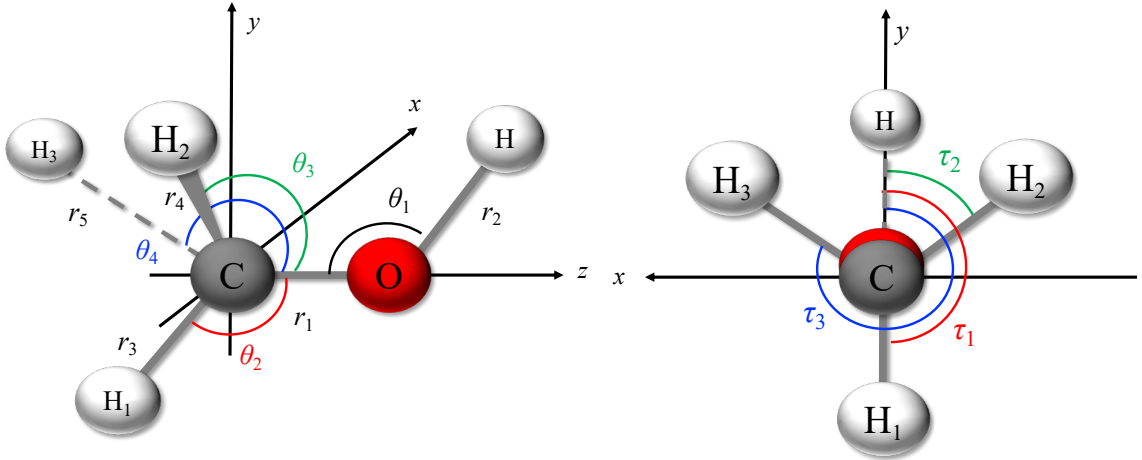


FIG. 1. Definition of the primitive internal coordinates of the methanol molecule and the body-fixed Cartesian frame used in this work.

TABLE IV. Harmonic frequencies and harmonic zero-point vibrational energy (ZPVE) in cm^{-1} at one of the three permutationally equivalent equilibrium structures and one saddle point obtained with the PES25 and *ab initio* computations. The harmonic frequencies of Ref. 59 are listed in decreasing energetic order. Mean absolute errors (MAE) and maximum (MAX) errors of the harmonic frequencies computed with the PESs and obtained from the *ab initio* computations are also shown.

description	coord	sym	Equilibrium structure				Saddle point			
			this work		Ref. 59		this work		Ref. 59	
			PES25	<i>ab initio</i> ^a	PES13	<i>ab initio</i> ^b	PES25	<i>ab initio</i> ^a	PES13	<i>ab initio</i> ^b
$\nu(\text{OH})$	r_{OH}	a'	3863.1	3866.4	3869.5	3864.9	3898.5	3899.7	3901.8	3901.5
$\nu(\text{CH}_3)_{\text{asym}}$	r_{CH}	a'	3134.5	3136.7	3150.3	3133.0	3104.9	3107.7	3120.8	3106.1
$\nu(\text{CH}_3)_{\text{asym}}$	r_{CH}	a''	3073.1	3075.7	3068.8	3071.9	3093.8	3102.1	3090.2	3100.5
$\nu(\text{CH}_3)_{\text{sym}}$	r_{CH}	a'	3014.7	3015.9	3016.2	3013.4	3026.0	3029.1	3018.4	3029.6
$\delta(\text{CH}_3)_{\text{asym}}$	φ_2	a'	1525.0	1521.6	1527.1	1514.8	1528.1	1529.1	1518.4	1526.8
$\delta(\text{CH}_3)_{\text{asym}}$	φ_1	a''	1512.5	1511.1	1499.0	1504.6	1505.6	1500.8	1508.6	1499.2
$\delta(\text{CH}_3)_{\text{sym}}$	θ_{HCO}	a'	1485.5	1485.4	1476.0	1481.3	1487.8	1489.4	1498.2	1487.7
$\delta(\text{COH})$	θ_{COH}	a'	1378.9	1383.7	1376.8	1380.5	1356.0	1366.3	1369.0	1366.0
$\rho(\text{CH}_3)$	θ_{HCO}	a''	1177.8	1181.7	1196.2	1178.4	1186.5	1191.5	1191.4	1192.3
$\rho(\text{CH}_3)$	θ_{HCO}	a'	1092.0	1090.1	1067.0	1089.5	1097.4	1096.8	1080.3	1100.3
$\nu(\text{CO})$	r_{CO}	a'	1063.3	1062.2	1065.2	1064.3	1062.2	1063.1	1058.5	1069.1
tor(OH)	τ	a''	298.6	293.1	287.0	289.2	300.8 <i>i</i>	295.6 <i>i</i>	301.9 <i>i</i>	284.8 <i>i</i>
ZPVE			11309.6	11311.8	11299.6	11292.9	11173.5	11187.8	11177.8	11189.6
MAE			2.6		8.2		3.7		9.7	
MAX			5.5		22.5		10.3		20.0	

^a CCSD(T)-F12b/cc-pVTZ-F12 ^b CCSD(T)-F12b/aug-cc-pVDZ

III. VARIATIONAL VIBRATIONAL COMPUTATIONS

A. Methodological details

We solve the vibrational Schrödinger equation,

$$[\hat{T}^v + V]\Psi_n = E_n\Psi_n \quad (3)$$

using the V potential energy surface developed in the first part of this work. The vibrational kinetic energy operator is

$$\hat{T}^v = -\frac{\hbar^2}{2} \sum_{k=1}^D \sum_{l=1}^D G_{kl} \frac{\partial}{\partial \rho_k} \frac{\partial}{\partial \rho_l} - \frac{\hbar^2}{2} \sum_{k=1}^D B_k \frac{\partial}{\partial \rho_k} + U \quad (4)$$

with

$$B_k = \sum_{l=1}^D \frac{\partial}{\partial \rho_l} G_{lk} \quad (5)$$

and

$$U = \frac{\hbar^2}{32} \sum_{k=1}^D \sum_{l=1}^D \left[\frac{G_{kl}}{\tilde{g}^2} \frac{\partial \tilde{g}}{\partial \rho_k} \frac{\partial \tilde{g}}{\partial \rho_l} + 4 \frac{\partial}{\partial \rho_k} \left(\frac{G_{kl}}{\tilde{g}} \frac{\partial \tilde{g}}{\partial \rho_l} \right) \right], \quad (6)$$

where D is the vibrational dimensionality (here $D = 12$), $\tilde{g} = \det \mathbf{g}$ is the determinant and $G_{kl} = (\mathbf{g}^{-1})_{kl}$ labels elements of the inverse of the mass-weighted metric tensor corresponding to the coordinate transformation from laboratory-frame Cartesian coordinates to rotational and internal, vibrational coordinates (the overall molecular translation is exactly separated⁴⁴).

The ρ_k internal coordinate definition is summarised as follows. To have a large-amplitude torsional coordinate that carries the permutation symmetry of the three hydrogens of the methyl unit, we define the following linear combinations of the τ_1, τ_2 and τ_3 primitive dihedral angles (Fig. 1)^{50,76,77},

$$\tau = \frac{1}{3} (\tau_1 + \tau_2 + \tau_3), \quad (7)$$

$$\varphi_1 = \frac{1}{\sqrt{2}} (\tau_2 - \tau_3), \quad (8)$$

$$\varphi_2 = \frac{1}{\sqrt{6}} (2\tau_1 - \tau_2 - \tau_3). \quad (9)$$

The dynamically relevant interval for τ is $[0, 2\pi)$; φ_1 and φ_2 are small-amplitude coordinates. To describe the small-amplitude vibrations, we start with the bond distances and angles of the valence coordinates (Fig. 1) and add φ_1 and φ_2 of Eqs. (8)–(9),

$$\boldsymbol{\xi} = (r_1, r_2, r_3, r_4, r_5, \theta_1, \theta_2, \theta_3, \theta_4, \varphi_1, \varphi_2). \quad (10)$$

Then, we define the q_k curvilinear normal coordinates by the linear combination of the $D^s = 11$ small-amplitude coordinates as

$$\Delta \xi_i = \sum_{k=1}^{D^s} L_{ik} q_k \quad \text{with} \quad \Delta \xi_i = \xi_i - \xi_i^{\text{ref}}(\tau), \quad i = 1, \dots, D^s. \quad (11)$$

$\boldsymbol{\xi}^{\text{ref}}(\tau)$ is the minimum-energy path on the PES for τ . \mathbf{L} diagonalizes the $\bar{\mathbf{G}}^s \bar{\mathbf{F}}^s$ matrix, where $\bar{\mathbf{G}}^s$ and $\bar{\mathbf{F}}^s$ are obtained by averaging the elements of the $D^s \times D^s$ $\mathbf{G}^s(\tau_i)$ matrix and the $\mathbf{F}^s(\tau_i)$ force-constant matrix over the three minimum structures, $\tau = \pi/3, \pi, 5\pi/3$. Eq. 11 defines the small-amplitude q_k coordinates, and so, the vibrational coordinates used in the vibrational kinetic energy operator, Eq. (4), are $\boldsymbol{\rho} = (q_1, \dots, q_{D^s}; \tau)$. As a result of this construction, the coupling of the small-amplitude coordinates is small (at the harmonic level), and thus, we can use an efficient basis and grid pruning. Further details (and possible coordinate choices) are described in Ref. 58. We note that the $\boldsymbol{\xi}^{\text{ref}}(\tau)$ minimum-energy path and the \mathbf{L} coefficients were (re-)computed with the PES25 developed in the first part of this work, the associated harmonic frequencies are provided in the ESI (Table S5).

We solve Eq. (3) in a variational procedure; harmonic oscillator basis functions are used for the q_k small-amplitude degrees of freedom, and Fourier basis functions for the τ large-amplitude motion. A direct product basis representation would be too large for this 12D system, so we exploit that the

TABLE V. Deviation of the vibrational band origins, $\tilde{\nu}$, in cm^{-1} , of CH_3OH computed with the GENIUSH-Smolyak program with PES13⁵⁹ and PES25 (this work) from available experimental data.

Description	Energy range [cm^{-1}]	$\tilde{\nu}$ (PES13) ⁵⁸			$\tilde{\nu}$ (PES25)		
		MAE	RMSE	MAX	MAE	RMSE	MAX
(a) torsional excitations:	0–1050	1.6	1.9	3.2	0.9	1.1	2.1
(b) SAM-torsion couplings:	1050–2000	6.9	8.4	16.1	1.5	2.0	4.0
(c) combination bands:	2000–2200	9.3	11.9	21.3	1.5	1.8	3.2

coupling of the small-amplitude vibrations is small^{44,56–58} and we can truncate the direct-product basis. For the computation of the Hamiltonian matrix, we use the Smolyak non-product grid to numerically compute integrals for the small-amplitude coordinates^{52–54,57,78,79}. The \mathbf{g} matrix and all further kinetic energy coefficients are computed over the multi-dimensional grid of the vibrational coordinates (q_k and τ) and the t -vector formalism is used as described in Refs. 44,80 and 52. Regarding the number of basis functions and grid points, extensive convergence tests on a former PES have been reported in Ref. 58. In this work, the following basis and grid parameters are used in the GENIUSH-Smolyak computation (the definition of these computational parameters can be found in Refs. 52,53,56–58): $n_\tau = 32$ and $M_\tau = 54$ for the LAM basis and grid size; and $b = 7$ and $H = 21$ for the SAM basis truncation and grid pruning which converge the vibrational energies within 0.5 cm^{-1} up to 2000 cm^{-1} from the ZPVE and within 1.5 cm^{-1} up to 2200 cm^{-1} .

B. Vibrational energies

First of all, we compare the vibrational energies computed with the newly developed PES25, and with the previously available PES13⁵⁹. For the comparison, we match the vibrational states based on their assignment, and this assignment also helps us compare with data from the (gas-phase) experiment. The vibrational energies and assignments with PES13 are taken from Ref. 58, and the new, detailed assignments with PES25 are collected in Tables S6-S8 of the ESI. The mean absolute error (MAE), root mean square error (RMSE), and maximum error (MAX) resulting from this analysis are shown in Table V.

The comparison, in Table V, is shown over three energy ranges defined according to the vibrational excitation types: (a) torsional states, $0\text{--}1050 \text{ cm}^{-1}$; (b) vibration-torsion coupling states, $1050\text{--}1600 \text{ cm}^{-1}$; and (c) combination bands, $2000\text{--}2200 \text{ cm}^{-1}$. To prepare Table V, only gas-phase experimental data were used. There are further, matrix-isolation vibrational band origins in neon and nitrogen matrices available in the literature. They are included in Table S8, and the agreement is mostly good with our variational results. However, direct, quantitative comparison (as for gas-phase data) is hindered by unpredictable matrix effects, which may be larger than the inaccuracy of our computations.

We also report that while the computed and experimental vibrational band origins (VBOs) are within a few cm^{-1} with PES13 or PES25 for the lowest-energy (a) range; the RMSE (MAX) of the VBOs with PES13 increases to 12 (21) cm^{-1} for PES13 for the combination band range (c). At the same time, for the newly developed PES25, the RMSE (MAX) of VBOs remain small, and even for the large-energy (c) range, they are only 1.8 (3.2) cm^{-1} , far lower than the RMS fitting errors of the fitting set of PES25.

The computed VBOs using PES25 and the error from the available experiment are listed in Table VI.

There are several VBOs, for which there is currently no (gas-phase) experimental value available. For an overall assessment, we compare the VBOs of the PES13 and PES25 in Figure 2, which reveals large, $> 10 \text{ cm}^{-1}$, deviations beyond ca. 1500 cm^{-1} . The figure also shows the deviations from the gas-phase experimental data summarised in Table V.

These observations suggest that PES25 represents a major improvement over earlier PES representations and provides a (near) spectroscopic quality description not only for the torsional excitation range but also for the vibration-torsion coupling and combination bands. Hence, it sets the ground for further vibrational and rovibrational computations.

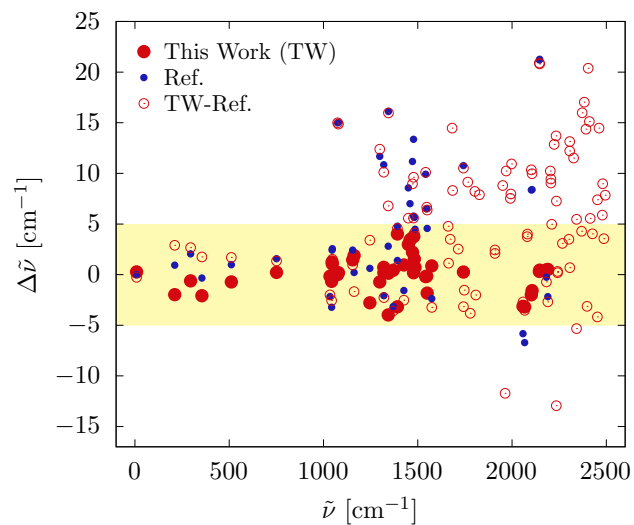


FIG. 2. Variational vibrational band origins computed in this work, with the newly developed PES25, at the CCSD(T)-F12b/cc-pVTZ-F12 level of electronic structure theory and the GENIUSH-Smolyak program, reproduce experimental data with $\Delta\tilde{\nu}$ difference less than $\pm 5 \text{ cm}^{-1}$. They significantly improve upon earlier results (Ref.) computed with PES13⁵⁹ and reported in Ref. 58. The vibrational band origins are referenced to the ZPVE of each computation. The ZPVEs with the PES13 and the PES25 are 11108.0 cm^{-1} ¹⁵⁸ and 11119.6 cm^{-1} (this work).

TABLE VI. Variational vibrational energies, $\tilde{\nu}$ in cm^{-1} , referenced to the zero-point vibrational energy (ZPVE, 11119.6 cm^{-1}) of CH_3OH in 12D computed with the GENIUSH-Smolayk program ($b = 7$ basis set) and PES25 developed in the present work.

#	ν_τ^a	SAMs ^b	Γ^c	$\tilde{\nu}$	δ^d	#	ν_τ^a	SAMs ^b	Γ^c	$\tilde{\nu}$	δ^d	#	ν_τ^a	SAMs ^b	Γ^c	$\tilde{\nu}$
1	0	0	A_1	0		51-52	2	8_1	E	1549.9	[-1.8]	103-104	3	5_1	E	2203.0
2-3	0	0	E	8.9	[0.3]	53-54	1	6_1	E	1574.5	[0.9]	105	3	$4_1, 10_1$	A_2	2205.8
4-5	1	0	E	210.9	[-2.0]	55-56	1,2	$5_1, 7_1, 11_1$	E	1661.1		106	3	$4_1, 10_1$	A_1	2206.2
6	1	0	A_2	295.1	[-0.6]	57-58	1	5_1	E	1663.9		107-108	3,4	$7_1, 11_1$	E	2210.4
7	2	0	A_1	355.3	[-2.1]	59	1	$4_1, 10_1$	A_2	1672.2		109-110	0	$7_2, 11_2$	E	2223.8
8-9	2	0	E	511.0	[-0.7]	60	1	$4_1, 10_1$	A_1	1682.5		111	0,1	mix	A_2	2233.7
10-11	3	0	E	750.8	[0.2]	61-62	1	$4_1, 10_1$	E	1685.0		112-113	3,4	$7_1, 11_1$	E	2234.6
12	0	8_1	A_1	1034.5	[-0.2]	63	1,2	$6_1, 7_1, 11_1$	A_2	1714.7		114-115	3	$4_1, 10_1$	E	2235.1
13-14	0	8_1	E	1043.3	[-0.7]	64	2	$6_1, 7_1, 11_1$	A_1	1742.2		116	5	0	A_2	2241.4
15	3	0	A_2	1045.4	[1.2]	65-66	2	6_1	E	1742.4	[0.3]	117	6	0	A_1	2241.5
16	4	0	A_1	1046.5	[1.1]	67	1	5_1	A_2	1746.6		118-119	1	8_2	E	2267.5
17	0	$6_1, 7_1, 11_1$	A_1	1074.7	[0.0]	68-69	1	$4_1, 10_1$	E	1765.1		120	0	mix	A_1	2301.6
18-19	0	$6_1, 7_1, 11_1$	E	1079.1	[0.2]	70-71	3	8_1	E	1778.5		121	4	6_1	A_1	2306.2
20-21	0	$7_1, 11_1$	E	1155.0	[1.5]	72-73	5	0	E	1803.0		122	3	6_1	A_2	2306.2
22	0	$7_1, 11_1$	A_2	1162.1	[1.9]	74	2	5_1	A_1	1807.7		123-124	0	mix	E	2306.3
23-24	1	8_1	E	1245.8	[-2.8]	75-76	2	$4_1, 10_1$	E	1827.1		125-126	0	mix	E	2326.3
25-26	0	6_1	E	1298.2	[-0.7]	77	3	$7_1, 11_1$	A_1	1909.7		127	1	8_2	A_2	2342.2
27	0,1	$6_1, 7_1, 11_1$	A_1	1319.9	[0.7]	78	3	$7_1, 11_1$	A_2	1909.8		128	0	mix	A_1	2342.3
28	1	$7_1, 8_1, 11_1$	A_2	1320.4	[0.2]	79-80	2,3	$6_1, 7_1, 11_1$	E	1950.9		129-130	1	mix	E	2368.8
29-30	1	6_1	E	1343.5	[-4.0]	81-82	2	5_1	E	1963.1		131	1	8_2	A_2	2372.0
31	1	8_1	A_2	1344.9	[0.1]	83-84	2	$4_1, 10_1$	E	1969.1		132	0	6_2	A_1	2383.6
32	0,2	$6_1, 7_1, 11_1$	A_1	1369.3	[0.4]	85	2	$4_1, 10_1$	A_2	1991.2		133-134	0,1	$6_2, 7_2, 11_2$	E	2392.3
33	2	8_1	A_1	1392.1	[-3.2]	86	2	$4_1, 10_1$	A_1	1993.8		135	0	mix	A_1	2397.9
34-35	4	0	E	1392.2	[4.0]	87-88	3	6_1	E	1997.5		136	0	mix	A_2	2403.9
36-37	1	$7_1, 11_1$	E	1426.2	[1.0]	89	0	8_2	A_1	2058.1	[-3.1]	137-138	0,1	$6_2, 7_2, 11_2$	E	2410.4
38	0	5_1	A_1	1450.3	[3.0]	90-91	0	8_2	E	2066.8	[-3.2]	139	2	8_2	A_1	2414.9
39-40	0	5_1	E	1458.7	[3.4]	92	3	8_1	A_2	2080.9		140-141	4	8_1	E	2426.6
41-42	0	$4_1, 10_1$	E	1471.7	[2.2]	93	4	8_1	A_1	2081.9		142-143	1	mix	E	2452.6
43-44	2	$7_1, 11_1$	E	1477.4		94	0	mix	A_1	2102.2	[-2.0]	144	1	mix	A_1	2453.4
45	0	$4_1, 10_1$	A_2	1477.8	[3.7]	95-96	0	mix	E	2106.4	[-1.6]	145-146	0	mix	E	2461.5
46-47	0	$4_1, 10_1$	E	1481.8	[1.5]	97	0	mix	A_1	2144.8	[0.3]	147	0	$5_1 + 8_1$	A_1	2478.9
48	0	$4_1, 10_1$	A_1	1485.4	[0.7]	98-99	0	mix	E	2146.9	[0.4]	148	0,1	mix	A_2	2481.0
49	1	6_1	A_2	1541.7	[-0.2]	100-101	0	mix	E	2182.5	[0.5]	149	0	$5_1 + 8_1$	E	2487.2
50	2	6_1	A_1	1547.4	[-0.1]	102	0	mix	A_2	2190.1	[0.5]	150	0,2	mix	E	2494.3

^a Assignment of the torsional excitation similarly to Ref. 58.

^b Assignment in terms of the (small-amplitude, SAM) curvilinear normal modes $1_n, 2_n, \dots, 11_n$ ($n = 0, 1, \dots$). Zero excitation ($n = 0$) is noted as '0'. The label 'mix' stands for strongly mixed states.

^c Γ : $C_{3v}(M)$ irreducible representation label. Further details are in Sec. S1 of the Supporting Information of Ref. 58.

^d Deviation from the experimental vibrational band origin^{19,22-24,81,82}, $\delta = \tilde{\nu}_{\text{exp}} - \tilde{\nu}$ in cm^{-1} . Gas-phase experimental data were not available to us for the states #103-150. Matrix-isolation data are cited in Table S8.

IV. SUMMARY, CONCLUSION, AND OUTLOOK

We have reported the development of an *ab initio* potential energy surface and variational vibrational states for the methanol molecule.

The electronic structure computations were carried out at the CCSD(T)-F12b/cc-pVTZ-F12 level of theory, the dataset for the PES was generated with the ROBOSURFER code, and the PES was fitted using the permutationally invariant polynomials (PIP) method. Properties of the PES, including molecular structure parameters, harmonic frequencies, and one-dimensional slices, were thoroughly investigated, and all details reproduce the *ab initio* values well.

The vibrational states of methanol were computed using this newly developed PES and the GENIUSH-Smolyak approach up to the coupling between the torsion and the overtone of the C-O stretching vibration (ca. 2500 cm^{-1} beyond the zero-point vibrational energy). The resulting vibrational band origins improve upon, by $10\text{-}20\text{ cm}^{-1}$, earlier vibrational results (computed on PES13) and are in good agreement ($\pm 5\text{ cm}^{-1}$) with available gas-phase experimental data. In the variational vibrational computations, we have confirmed that the vibrational energies are converged within $1\text{-}2\text{ cm}^{-1}$ with respect to the vibrational basis for these ranges.

As a result, we describe the quantum dynamics of methanol here using a fully *ab initio* approach, confirmed with experiment from the torsional excitation range, through the vibration-torsion coupling, up to the start of the combination bands range at around 2500 cm^{-1} beyond the zero-point vibrational energy. This result opens the door for future rovibrational computations, for which we plan to implement a path-following, body-fixed frame approach. Furthermore, the development of electric dipole and polarizability surfaces is in progress. This will allow us a fully *ab initio* computation and line-by-line study of the high-resolution infrared and Raman spectra. All in all, the present work is an important step towards simulating the ‘complete’ rovibrational spectrum of methanol (and isotopologues) for further applications in astrochemistry, astrophysics, and fundamental physics.

ACKNOWLEDGMENTS

AS thanks the European Union’s Horizon 2022 research and innovation programme under the Marie Skłodowska-Curie Grant Agreement No. 101105452 (QDMAP). AS and EM thank the financial support of the Hungarian National Research, Development, and Innovation Office (FK 142869). TG and GC thank the National Research, Development and Innovation Office-NKFIH, K-146759; project no. TKP2021-NVA-19, provided by the Ministry of Culture and Innovation of Hungary from the National Research, Development and Innovation Fund, financed under the TKP2021-NVA funding scheme; and the Momentum (Lendület) Program of the Hungarian Academy of Sciences for financial support. We acknowledge KIFÜ (Governmental Agency for IT Development, Hungary) for awarding us access to the Komondor HPC facility based in Hungary. We thank Viktor Tajti (Szeged) for the extension of the QCT MD code to compute unimolecular trajectories.

-
- [1] P. Jansen, L.-H. Xu, I. Kleiner, W. Ubachs, and H. L. Bethlem, Methanol as a sensitive probe for spatial and temporal variations of the proton-to-electron mass ratio, *Phys. Rev. Lett.* **106**, 100801 (2011).
 - [2] S. A. Levshakov, M. G. Kozlov, and D. Reimers, Methanol as a tracer of fundamental constants, *ApJ* **738**, 26 (2011).
 - [3] J. Bagdonaite, P. Jansen, C. Henkel, H. Bethlem, K. Menten, and W. Ubachs, A stringent limit on a drifting proton-to-electron mass ratio from alcohol in the early universe, *Science* **339**, 46 (2013).
 - [4] J. S. Vorotyntseva, M. G. Kozlov, and S. A. Levshakov, Methanol isotopologues as a probe for spatial and temporal variations of the electron-to-proton mass ratio, *Mon. Not. R. Astron. Soc.* **527**, 2750 (2023).
 - [5] A. Sunaga, Strong parity-violation effects induced by large-amplitude motions: A quantum-dynamics study of substituted chiral methanols, *J. Chem. Phys.* **162**, 064302 (2025).
 - [6] B. Lankhaar, W. Vlemmings, G. Surcis, H. J. van Langevelde, G. C. Groenenboom, and A. van der Avoird, Characterization of methanol as a magnetic field tracer in star-forming regions, *Nat. Astron.* **2**, 145 (2018).

- [7] I. Kleiner, Spectroscopy of interstellar internal rotors: An important tool for investigating interstellar chemistry, *ACS Earth Space Chem.* **3**, 1812 (2019).
- [8] J. K. Jørgensen, M. H. D. van der Wiel, A. Coutens, J. M. Lykke, H. S. P. Müller, E. F. van Dishoeck, H. Calcutt, P. Bjerke, T. L. Bourke, M. N. Drozdovskaya, C. Favre, E. C. Fayolle, R. T. Garrod, S. K. Jacobsen, K. I. Öberg, M. V. Persson, and S. F. Wampfler, The ALMA protostellar interferometric line survey (PILS): First results from an unbiased submillimeter wavelength line survey of the class 0 protostellar binary IRAS 16293-2422 with ALMA, *Astron. Astrophys.* **595**, A117 (2016).
- [9] T. Oyama, Y. Ohno, A. Tamanai, Y. Watanabe, S. Yamamoto, T. Sakai, S. Zeng, R. Nakatani, and N. Sakai, Laboratory measurement of CH₂DOH line intensities in the millimeter-wave region, *Astrophys. J.* **957**, 4 (2023).
- [10] W. Riedel, O. Sipilä, E. Redaelli, P. Caselli, A. I. Vasyunin, F. Dulieu, and N. Watanabe, Modelling deuterated isotopologues of methanol towards the pre-stellar core L1544, *Astron. Astrophys.* **680**, A87 (2023).
- [11] J.-H. Jeong, J.-E. Lee, S. Lee, G. Baek, J.-H. Kang, S. Lee, C.-H. Kim, H.-S. Yun, Y. Aikawa, G. J. Herczeg, D. Johnstone, and L. Cieza, ALMA spectral survey of an eruptive young star, V883 ori (ASSAY). II. freshly sublimated complex organic molecules in the keplerian disk, *Astrophys. J. Suppl. Ser.* **276**, 49 (2025).
- [12] A. Tamanai, T. Oyama, Y. Watanabe, T. Sakai, R. Nakatani, S. Zeng, I. Kleiner, and N. Sakai, Laboratory measurement of CH₃¹⁷OH transitions in the frequency range from 216 to 264 GHz for astronomical application, *Astrophys. J.* **980**, 110 (2025).
- [13] A. Borden and E. F. Barker, The infra-red absorption spectrum of methyl alcohol, *J. Chem. Phys.* **6**, 553 (1938).
- [14] J. O. Halford, L. C. Anderson, and G. H. Kissin, The raman spectra of the methyl alcohols, CH₃OH, CH₃OD, and CH₂DOD, *J. Chem. Phys.* **5**, 927 (1937).
- [15] C. Tanaka, K. Kuratani, and S.-I. Mizushima, In-plane normal vibrations of methanol, *Spectrochim. Acta* **9**, 265 (1957).
- [16] M. Falk and E. Whalley, Infrared spectra of methanol and deuterated methanols in gas, liquid, and solid phases, *J. Chem. Phys.* **34**, 1554 (1961).
- [17] A. Timidei and G. Zerbi, Valence force constants and normal vibrations of methanol, *Z. Naturforsch. A* **25**, 1729 (1970).
- [18] T. Shimanouchi, *Tables of Molecular Vibrational Frequencies Consolidated, vol. 1* (Nat. Stand. Ref. Data Ser., Nat. Bur. Stand. (U.S.), 1972).
- [19] A. Serrallach, R. Meyer, and H. Günthard, Methanol and deuterated species: Infrared data, valence force field, rotamers, and conformation, *J. Mol. Spectrosc.* **52**, 94 (1974).
- [20] E. Herbst, J. K. Messer, and F. C. de Lucia, A new analysis and additional measurements of the millimeter and submillimeter spectrum of methanol, *J. Mol. Spectrosc.* **108**, 42 (1984).
- [21] L.-H. Xu, M. S. Walsh, and R. M. Lees, Global fit of torsion – rotation transitions in the ground and first excited torsional states of ¹³C-Methanol, *J. Mol. Spectrosc.* **179**, 269 (1996).
- [22] R. M. Lees, M. Mollabashi, L.-H. Xu, M. Lock, and B. P. Winnewisser, Variations in the torsion-vibration energy structure of CH₃OH from fundamental, overtone, and combination bands of the ν_7, ν_8 and ν_{11} CH₃ rocking and CO stretching modes, *Phys. Rev. A* **65**, 042511 (2002).
- [23] R. M. Lees, L.-H. Xu, J. W. C. Johns, Z.-F. Lu, B. P. Winnewisser, M. Lock, and R. L. Sams, Fourier transform spectroscopy of CH₃OH: rotation–torsion–vibration structure for the CH₃-rocking and OH-bending modes, *J. Mol. Spectrosc.* **228**, 528 (2004).
- [24] M. Abouti Tamsamani, L.-H. Xu, and R. M. Lees, A rotation–torsion–vibration treatment with three-dimensional internal coordinate approach and additional FTIR spectral assignments for the CH₃-bending fundamentals of methanol, *J. Mol. Spectrosc.* **218**, 220 (2003).
- [25] L.-H. Xu, J. Fisher, R. M. Lees, H. Y. Shi, J. T. Hougen, J. C. Pearson, B. J. Drouin, G. A. Blake, and R. Braakman, Torsion–rotation global analysis of the first three torsional states ($\nu_t = 0, 1, 2$) and terahertz database for methanol, *J. Mol. Spectrosc.* **251**, 305 (2008).
- [26] R. Santagata, D. B. A. Tran, B. Argence, O. Lopez, S. K. Tokunaga, F. Wiotte, H. Mouhamad, A. Goncharov, M. Abgrall, Y. Le Coq, H. Alvarez-Martinez, R. Le Targat, W. K. Lee, D. Xu, P.-E. Pottie, B. Darquié, and A. Amy-Klein, High-precision methanol spectroscopy with a widely tunable SI-traceable frequency-comb-based mid-infrared QCL, *Optica* **6**, 411 (2019).
- [27] P. R. Bunker and P. Jensen, *Molecular Symmetry and Spectroscopy, 2nd Ed* (NRC Research Press, 2006).
- [28] M. Quack, Detailed symmetry selection rules for reactive collisions, *Mol. Phys.* **34**, 477 (1977).
- [29] M. Quack and F. Merkt, *Handbook of High-resolution Spectroscopy* (John Wiley & Sons, 2011).
- [30] J. P. Perchard, The torsion-vibration spectrum of methanol trapped in neon matrix, *Chem. Phys.* **332**, 86 (2007).
- [31] J. P. Perchard, F. Romain, and Y. Bouteiller, Determination of vibrational parameters of methanol from matrix-isolation infrared spectroscopy and ab initio calculations. part 1 – spectral analysis in the domain 11000–200 cm⁻¹, *Chem. Phys.* **343**, 35 (2008).
- [32] D. F. Dinu, K. Oenen, J. Schlagin, M. Podewitz, H. Grothe, T. Loerting, and K. R. Liedl, How

- vibrational notations can spoil infrared spectroscopy: A case study on isolated methanol, *ACS Phys. Chem. Au* **4**, 679 (2024).
- [33] J. M. Bowman, Self-consistent field energies and wavefunctions for coupled oscillators, *J. Chem. Phys.* **68**, 608 (1978).
- [34] K. Yagi, K. Hirao, T. Taketsugu, M. W. Schmidt, and M. S. Gordon, Ab initio vibrational state calculations with a quartic force field: applications to H_2CO , C_2H_4 , CH_3OH , CH_3CCH , and C_6H_6 , *J. Chem. Phys.* **121**, 1383 (2004).
- [35] F. Partal Ureña, J. J. López González, and F. Márquez, Anharmonic spectra of methanol and silanol: A comparative study, *J. Mol. Spectrosc.* **233**, 203 (2005).
- [36] Y. Scribano, D. M. Lauvergnat, and D. M. Benoit, Fast vibrational configuration interaction using generalized curvilinear coordinates and self-consistent basis, *J. Chem. Phys.* **133**, 094103 (2010).
- [37] B. Schröder and G. Rauhut, Vibrational configuration interaction theory, in *Vibrational Dynamics of Molecules* (WORLD SCIENTIFIC, 2022) pp. 1–40.
- [38] D. F. Dinu, M. Podewitz, H. Grothe, T. Loerting, and K. R. Liedl, On the synergy of matrix-isolation infrared spectroscopy and vibrational configuration interaction computations, *Theor. Chem. Acc.* **139**, 174 (2020).
- [39] H. R. Larsson, Benchmarking vibrational spectra: 5000 accurate eigenstates of acetonitrile using tree tensor network states, *J. Phys. Chem. Lett.* , 3991 (2025).
- [40] A. G. Császár, C. Fábri, T. Szidarovszky, E. Mátyus, T. Furtenbacher, and G. Czako, The fourth age of quantum chemistry: molecules in motion, *Phys. Chem. Chem. Phys.* **14**, 1085 (2012).
- [41] J. Tennyson, Perspective: Accurate ro-vibrational calculations on small molecules, *J. Chem. Phys.* **145**, 120901 (2016).
- [42] T. Carrington, Jr, Perspective: Computing (ro-)vibrational spectra of molecules with more than four atoms, *J. Chem. Phys.* **146**, 120902 (2017).
- [43] A. Chen, A. Nauts, and D. Lauvergnat, ElVibRot-MPI: parallel quantum dynamics with smolyak algorithm for general molecular simulation, *arXiv [physics.comp-ph]* (2021), [arXiv:2111.13655 \[physics.comp-ph\]](https://arxiv.org/abs/2111.13655).
- [44] E. Mátyus, A. Martín Santa Daría, and G. Avila, Exact quantum dynamics developments for floppy molecular systems and complexes, *Chem. Commun.* **59**, 366 (2023).
- [45] J. Simmons and T. Carrington, Jr, Computing vibrational spectra using a new collocation method with a pruned basis and more points than basis functions: Avoiding quadrature, *J. Chem. Phys.* **158**, 144115 (2023).
- [46] R. Wodraszka and T. Carrington, Jr, Using a pruned basis and a sparse collocation grid with more points than basis functions to do efficient and accurate MCTDH calculations with general potential energy surfaces, *J. Chem. Phys.* **160**, 214121 (2024).
- [47] S. D. Kallullathil and T. Carrington, Computing vibrational energy levels using a canonical polyadic tensor method with a fixed rank and a contraction tree, *J. Chem. Phys.* **158**, 214102 (2023).
- [48] I. Simkó, P. M. Felker, and Z. Bačić, HCl trimer: HCl-stretch excited intramolecular and intermolecular vibrational states from 12D fully coupled quantum calculations employing contracted intra- and intermolecular bases, *J. Chem. Phys.* **160**, 164304 (2024).
- [49] I. Simkó, P. Felker, and Z. Bačić, H_2O trimer: Rigorous 12D quantum calculations of intermolecular vibrational states, tunneling splittings, and low-frequency spectrum, *J. Chem. Phys.* **162**, 034301 (2025).
- [50] D. Lauvergnat and A. Nauts, Quantum dynamics with sparse grids: a combination of smolyak scheme and cubature. application to methanol in full dimensionality, *Spectrochim. Acta A Mol. Biomol. Spectrosc.* **119**, 18 (2014).
- [51] A. Nauts and D. Lauvergnat, Numerical on-the-fly implementation of the action of the kinetic energy operator on a vibrational wave function: application to methanol, *Mol. Phys.* **116**, 3701 (2018).
- [52] G. Avila and E. Mátyus, Toward breaking the curse of dimensionality in (ro)vibrational computations of molecular systems with multiple large-amplitude motions, *J. Chem. Phys.* **150**, 174107 (2019).
- [53] G. Avila and E. Matyus, Full-dimensional (12d) variational vibrational states of CH_4F^- : Interplay of anharmonicity and tunneling, *J. Chem. Phys.* **151**, 154301 (2019).
- [54] G. Avila, D. Papp, G. Czako, and E. Mátyus, Exact quantum dynamics background of dispersion interactions: case study for $\text{CH}_4\text{-Ar}$ in full (12) dimensions, *Phys. Chem. Chem. Phys.* **22**, 2792 (2020).
- [55] D. Papp, V. Tajti, G. Avila, E. Mátyus, and G. Czako, $\text{CH}_4\text{-F}^-$ revisited: full-dimensional ab initio potential energy surface and variational vibrational states, *Mol. Phys.* **121**, e2113565 (2023).
- [56] A. Martín Santa Daría, G. Avila, and E. Mátyus, Variational vibrational states of HCOOH , *J. Mol. Spectrosc.* **385**, 111617 (2022).
- [57] G. Avila, A. Martín Santa Daría, and E. Mátyus, Vibrational infrared and raman spectra of HCOOH from variational computations, *Phys. Chem. Chem. Phys.* **25**, 15183 (2023).
- [58] A. Sunaga, G. Avila, and E. Mátyus, Variational vibrational states of methanol (12D), *J. Chem. Theory Comput.* **20**, 8100 (2024).
- [59] C. Qu and J. M. Bowman, Full-dimensional, ab initio potential energy surface for $\text{CH}_3\text{OH} \rightarrow \text{CH}_3+\text{OH}$,

- Mol. Phys.* **111**, 1964 (2013).
- [60] X. Huang, B. J. Braams, and J. M. Bowman, Ab initio potential energy and dipole moment surfaces for H_5O_2^+ , *J. Chem. Phys.* **122**, 44308 (2005).
- [61] B. J. Braams and J. M. Bowman, Permutationally invariant potential energy surfaces in high dimensionality, *Int. Rev. Phys. Chem.* **28**, 577 (2009).
- [62] C. Qu, Q. Yu, and J. M. Bowman, Permutationally invariant potential energy surfaces, *Annual Review of Physical Chemistry* **69**, 151 (2018).
- [63] C. Qu, Q. Yu, B. L. Van Hoozen, Jr, J. M. Bowman, and R. A. Vargas-Hernández, Assessing gaussian process regression and permutationally invariant polynomial approaches to represent high-dimensional potential energy surfaces, *J. Chem. Theory Comput.* **14**, 3381 (2018).
- [64] D. R. Moberg and A. W. Jasper, Permutationally invariant polynomial expansions with unrestricted complexity, *J. Chem. Theory Comput.* **17**, 5440 (2021).
- [65] P. L. Houston, C. Qu, Q. Yu, R. Conte, A. Nandi, J. K. Li, and J. M. Bowman, PESPIP: Software to fit complex molecular and many-body potential energy surfaces with permutationally invariant polynomials, *J. Chem. Phys.* **158**, 044109 (2023).
- [66] M. S. Drehwald, A. Jamali, and R. A. Vargas-Hernández, MOLPIPx: An end-to-end differentiable package for permutationally invariant polynomials in python and rust, *J. Chem. Phys.* **162**, 084115 (2025), 2411.17011.
- [67] J. Bowman, C. Qu, R. Conte, A. Nandi, P. Houston, and Q. Yu, A perspective marking 20 years of using permutationally invariant polynomials for molecular potentials, ChemRxiv; doi:10.26434/chemrxiv-2025-v14p7 10.26434/chemrxiv-2025-v14p7 (2025).
- [68] T. Györi and G. Czakó, Automating the development of high-dimensional reactive potential energy surfaces with the robosurfer program system, *J. Chem. Theory Comput.* **16**, 51 (2020).
- [69] T. B. Adler, G. Knizia, and H.-J. Werner, A simple and efficient CCSD(T)-F12 approximation, *J. Chem. Phys.* **127**, 221106 (2007).
- [70] K. A. Peterson, T. B. Adler, and H.-J. Werner, Systematically convergent basis sets for explicitly correlated wavefunctions: the atoms H, He, B-Ne, and Al-Ar, *J. Chem. Phys.* **128**, 084102 (2008).
- [71] R. Lindh, U. Ryu, and B. Liu, The reduced multiplication scheme of the rys quadrature and new recurrence relations for auxiliary function based two-electron integral evaluation, *J. Chem. Phys.* **95**, 5889 (1991).
- [72] H.-J. Werner, P. J. Knowles, G. Knizia, F. R. Manby, and M. Schütz, Molpro: a general-purpose quantum chemistry program package, *Wiley Interdiscip. Rev. Comput. Mol. Sci.* **2**, 242 (2012).
- [73] H.-J. Werner, P. J. Knowles, F. R. Manby, J. A. Black, K. Doll, A. Heßelmann, D. Kats, A. Köhn, T. Korona, D. A. Kreplin, Q. Ma, T. F. Miller, 3rd, A. Mitrushchenkov, K. A. Peterson, I. Polyak, G. Rauhut, and M. Sibaev, The molpro quantum chemistry package, *J. Chem. Phys.* **152**, 144107 (2020).
- [74] H.-J. Werner, P. J. Knowles, P. Celani, W. Györfy, A. Hesselmann, D. Kats, G. Knizia, A. Köhn, T. Korona, D. Kreplin, R. Lindh, Q. Ma, F. R. Manby, A. Mitrushchenkov, G. Rauhut, M. Schütz, K. R. Shamasundar, T. B. Adler, R. D. Amos, S. J. Bennie, A. Bernhardsson, A. Berning, J. A. Black, P. J. Bygrave, R. Cimiraglia, D. L. Cooper, D. Coughtrie, M. J. O. Deegan, A. J. Dobbyn, K. Doll, M. Dornbach, F. Eckert, S. Erfort, E. Goll, C. Hampel, G. Hetzer, J. G. Hill, M. Hodges, T. Hrenar, G. Jansen, C. Köppl, C. Kollmar, S. J. R. Lee, Y. Liu, A. W. Lloyd, R. A. Mata, A. J. May, B. Mussard, S. J. McNicholas, W. Meyer, T. F. Miller III, M. E. Mura, A. Nicklass, D. P. O'Neill, P. Palmieri, D. Peng, K. A. Peterson, K. Pflüger, R. Pitzer, I. Polyak, M. Reiher, J. O. Richardson, J. B. Robinson, B. Schröder, M. Schwilk, T. Shiozaki, M. Sibaev, H. Stoll, A. J. Stone, R. Tarroni, T. Thorsteinsson, J. Toulouse, M. Wang, M. Welborn, and B. Ziegler, Molpro, version 2023.2, a package of ab initio programs, see <https://www.molpro.net>.
- [75] E. Anderson, Z. Bai, C. Bischof, S. Blackford, J. Demmel, J. Dongarra, J. Du Croz, A. Greenbaum, S. Hammarling, A. McKenney, and D. Sorensen, *LAPACK Users' Guide*, 3rd ed. (Society for Industrial and Applied Mathematics, Philadelphia, PA, 1999).
- [76] R. Meyer and H. H. Günthard, Internal rotation and vibration in $\text{CH}_2=\text{CCl}-\text{CH}_2\text{D}$, *J. Chem. Phys.* **50**, 353 (1969).
- [77] S. Bell, Variation of geometry, vibrational frequencies and zero-point energies with internal rotation, *J. Mol. Struct.* **320**, 125 (1994).
- [78] G. Avila and T. Carrington, Jr, Nonproduct quadrature grids for solving the vibrational schrodinger equation, *J. Chem. Phys.* **131**, 174103 (2009).
- [79] G. Avila and T. Carrington, Jr, Using nonproduct quadrature grids to solve the vibrational schrodinger equation in 12D, *J. Chem. Phys.* **134**, 054126 (2011).
- [80] E. Mátyus, G. Czakó, and A. G. Császár, Toward black-box-type full- and reduced-dimensional variational (ro)vibrational computations, *J. Chem. Phys.* **130**, 134112 (2009).
- [81] G. Moruzzi, B. P. Winnewisser, M. Winnewisser, I. Mukhopadhyay, and F. Strumia, *Microwave, Infrared, and Laser Transitions of Methanol Atlas of Assigned Lines from 0 to 1258 cm^{-1}* (CRC New York, 1995).
- [82] B. Fehrensen, D. Luckhaus, M. Quack, M. Willeke, and T. R. Rizzo, Ab initio calculations of mode

selective tunneling dynamics in $C^{12}H_3OH$ and $C^{13}H_3OH$, [J. Chem. Phys. **119**, 5534 \(2003\)](#).